Comparative Hydrodynamic Analysis of a Small Craft Hull Forms Using CFD

DOI: 10.25043/19098642.282

José S. Pájaro C. [1]
Omar D. Vásquez B. [2]

Abstract

The comparative assessment of hull forms remains a critical element in the optimization of small-craft design, particularly in terms of resistance and manoeuvering performance. This study presents a computational fluid dynamics (CFD) analysis of two hull configurations: a conventional bow and an alternative wide bow. Simulations were carried out in Star-CCM+ using a predefined velocity–heel–drift matrix, ensuring equal displacement for both hulls. The results are discussed with reference to hydrodynamic resistance and flow patterns. In addition, numerical outcomes at 6.50 knots without heel or drift were compared against the Delft Systematic Yacht Hull Series (DSYHS) to validate the computational approach. The findings highlight the influence of bow geometry on resistance characteristics and provide insight into the associated design trade-offs between seakeeping and efficiency. This research contributes to the understanding of hull optimization for naval applications, by offering a methodological framework for integrating CFD-based assessments with systematic experimental benchmarks.

Key words: Hull form comparison, hydrodynamic resistance, computational fluid dynamics, hydrodynamic simulation, Delft systematic yacht hull series, bow geometry.

How to cite this article

To cite this article, use the following format:

IEEE Format

[1] J. Pájaro and O. Vásquez, "Comparative Hydrodynamic Analysis of a Small Craft Hull Forms Using CFD" Ship Science and Technology (Cartagena), vol. 19, no. 37, pp. 41-51, 2025. DOI: https://doi.org/10.25043/19098642.282

Date Received: October 15th, 2025
Date Accepted: November 26th, 2025
Publication Date: December 20th, 2025

COTECMAR, Cartagena, Colombia. ROR: https://ror.org/01z04wv09
[1] Email: jspajaro@cotecmar.com ORCID: https://orcid.org/0009-0006-3941-0148
[2] Email: ovasquez@cotecmar.com ORCID: https://orcid.org/0009-0008-1798-8584

Introduction

The design of small craft presents challenges related to hy- drodynamic optimization, in which the hull form plays a decisive role in a vessel's overall performance. The geometry of the bow directly affects wave-making resistance, pressure distribution, and the way the hull behaves under heel and drift conditions. One notable example is the AXE Bow concept, which is characterized by a nearly vertical entry and a narrow frontal surface. This design reduces pitching and slamming, thereby improving seakeeping in adverse conditions *(Keuning et al., 2002)*. Subsequent studies have confirmed the advantages of this geometry compared to conventional designs, reporting lower resistance and improved dynamic responses in open sea conditions *(Rijkens and Mikelic, 2022)*.

In parallel, the application of Computational Fluid Dynamics (CFD) has become a fundamental tool for hull form analysis. These methods allow the prediction of resistance coefficients and flow patterns with improved accuracy and offer flexibility for evaluating multiple operational scenarios. For example, Domínguez Ruiz *et al*. (2020) analyzed six bow variants through CFD simulations and validated the results with experimental data from the Delft Systematic Yacht Hull Series, thereby demonstrating the reliability of numerical approaches in early-stage optimization studies.

More recently, Kazemi *et al*. (2021) applied CFD combined with artificial neural networks to predict the hydrodynamic performance of planing craft with different step configurations. Their results, validated against laboratory tests, highlighted the robustness of numerical methods and reinforced their appli- cability to complex geometrical arrangements. Furthermore, parametric optimization strategies such as Design of Experiments (DOE) and Response Surface Methodology (RSM) have achieved significant reductions —between 20% and 30%— in added resistance for bulk carriers, confirming the potential of combining CFD with statistical techniques for innovative bow design *(Matsumoto et al., 2019)*.

Within this framework, the present study aims to compare two hull configurations — one with a conventional bow and another with a wide bow— through CFD simulations performed in Star-CCM+. A test matrix including variations in speed, heel, and drift, while maintaining constant displacement, was defined to analyze resistance, flow patterns, and their correlation with reference values from the Delft Systematic Yacht Hull Series (DSYHS). This methodological approach builds on previous studies that demonstrate the predictive capability of CFD and its suitability for early-stage naval design *(Domínguez Ruiz et al., 2020; Kazemi et al., 2021).*

This work was developed as part of a project for the Small Vessel Design course in the ENAP naval engineering master's program, led by Dr. Richard Luco Salman.

Description of the problem

The design of small craft requires optimizing hydrodynamic efficiency while ensuring stability and maneuverability. Bow geometry plays a key role in this balance, as it strongly influences resistance, wave-making, and dynamic behavior under different operating conditions.

While conventional bows have been widely adopted, alternative configurations, such as wide bows, offer potential advantages in energy efficiency and seakeeping.

However, comparative evidence for these geometries remains limited particularly under scenarios combining variations in speed, heel, and drift.

This creates the need for a systematic analysis of the hydrodynamic performance

Table 1. Ship A Data Table.

Description	Symbol	Value
Length overall	L_{OA} (m)	12.00
Length between perpendiculars	L_{PP} (m)	11.97
Length of waterline	L_{WL} (m)	11.59
Maximum beam of waterline	B_{WL} (m)	3.47
Depth	D (m)	1.80
Draft	T (m)	0.46
Displacement volume	∇ (m^3)	7.79
Wetted surface area	S_W (m^2)	30.93
Block coefficient (C_B)	∇ /$LPP^{B}WL^{T}$	0.42
Prismatic coefficient (C_P)		0.57
Study Speeds	V (kn)	3.00/6.50/8.40

of conventional and wide-bow hulls, using CFD simulations validated against reference series such as Delft. The aim is to provide technical criteria that support design decisions that foster innovation and efficiency in small craft.

Geometry

The models used in this case study are part of the Delft Series; these hulls forms are intented solely for academic use Models A and B share identical principal dimensions; the only difference lies in their bow geometry.

Fig. 1. Type A sailboat (normal bow).

The geometry type A sailboat (normal bow) and a type B sailboat (wide bow):

Fig. 2. Type B sailboat (wide bow).

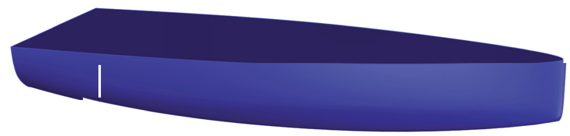

Table 2. Ship B Data Table.

Description	Symbol	Value
Length overall	L_{OA} (m)	12.00
Length between perpendiculars	L_{PP} (m)	11.89
Length of waterline	L_{WL} (m)	12.04
Maximum beam of waterline	B_{WL} (m)	3.46
Depth	D (m)	1.80
Draft	T (m)	0.46
Displacement volume	∇ (m^3)	7.77
Wetted surface area	S_W (m^2)	31.38
Block coefficient (C_B)	∇ /$LPP^{B}WL^{T}$	0.43
Prismatic coefficient (C_P)		0.57
Study Speeds	V (kn)	3.00/6.50/8.40

For this case, a comparative analysis was carried out on the behavior of these two types of hulls, based on hydrodynamic tests using CFD. the following properties were considered:

Table 3. Model conditions for analysis.

Speed (kn)	Heel (degrees)	Yaw (degrees)
3.00	0.00	0.00
6.50	0.00	0.00
6.50	15.00	1.50
8.40	0.00	0.00
8.40	15.00	2.50

Computational Domain

A fundamental part of any dynamic simulation is the correct definition of the domain conditions. In this study, despite using two vessel models (Types A and B), the domain volume is identical for simulations without heel and drift. This is because the main difference between the two models lies in the shape of the bow, while their principal dimensions—length, beam, and depth—are the same. These parameters are crucial for defining the control domain, as established in "Practical Guidelines for Ship CFD Applications."

As a result of applying these guidelines, the coordinates of the computational domain for simulations without heel and yaw are defined and presented in Table 4.

Table 4. Coordinates of the computational domain for simulations without heel and yaw.

Corner	x (m)	y (m)	z (m)
Corner 1	−24	−20	−12
Corner 2	24	0	12

The computational domain for the reference shown in Table 4 can be seen in Fig. 3.

Fig. 3. Computational domain for simulations without heel and yaw, models A y B.

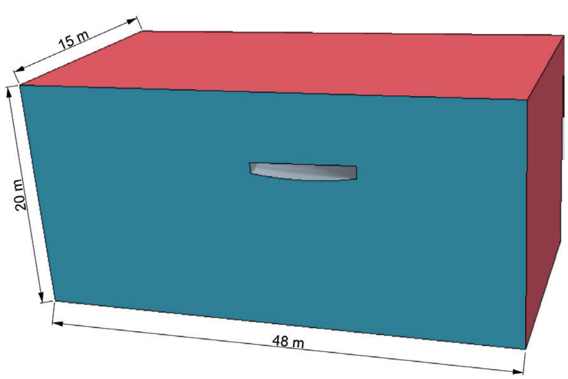

It is important to note that, while the domain maintains the same dimensions for simulations without heel and yaw, the approach varies significantly when either of these conditions is introduced. In simulations with heel or yaw, it is necessary to consider the full vessel for an accurate representation. Therefore, the computational domain must be extended, doubling on the Y-axis, to simulate the entire vessel. This is necessary to capture the effects of vessel motion and obtain results representative of real operating conditions. The coordinates that define this domain are indicated in Table 5.

Table 5. Coordinates of the computational domain for simulations with heel or yaw.

Corner	x (m)	y (m)	z (m)
Corner 1	−24	0	−12
Corner 2	24	15	8

These considerations, based on the "Practical Guidelines for Ship CFD Applications," were crucial for defining the appropri- ate domains according to the type of simulation.

Mesh Generation

The mesh used for both geometries was of the trimmer type. To parameterize the mesh, the length L = 12m was divided by he parameter R = 100, resulting in a base size (Bsize) of 0.12 m. (Fig. 4).

Fig. 4. Base Mesh for Models A and B.

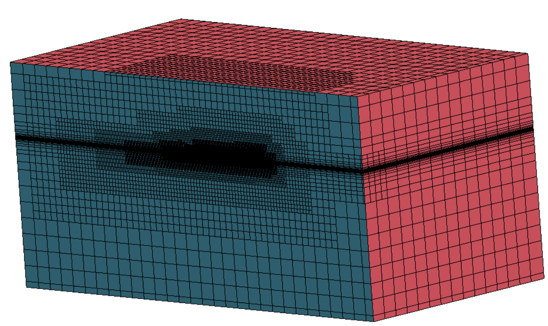

Refinements

Mesh refinement must be done considering the objective of the case study. In this case, it was essential to refine the mesh in key areas to ensure the accuracy of the results.

Specifically, refinements were applied to:

- **The bow**, to understand the behavior of the incoming flow.
- **The stern**, to analyze the outlet flow.
- **The free surface**, to capture the detailed interaction between the air, water, and the vessel.
- **The wake**, to observe the formed wave pattern.

The methodology for these refinements was based on the guidelines of the article "Speeding up Hydrodynamic Simulations with a Parametric, Templated Approach" Wheeler (2021), where control volumes are defined directly in relation to the vessel's principal dimensions, as illustrated in Fig. 5. The percentages and images of the applied refinement are shown in Table 6, Fig. 6, Fig. 7, and Fig. 8 respectively.

Table 6. Applied Meshing sizes as percentage of base size.

Parameter	x	y	z
Hull Surface	12.5	12.5	12.5
Hull Fine	200	200	100
Hull Coarse	400	400	200
Bow	6.25	6.25	6.25
Stern	12.5	12.5	12.5
Free Surface Fine	800	800	6.25
Free Surface Medium	800	800	25
Free Surface Coarse	800	800	50
Wake Fine	50	50	100
Wake Medium	100	100	100
Wake Coarse	200	200	200
Outer Boundaries	800	800	800

Fig. 5. Control volumes for mesh refinement.

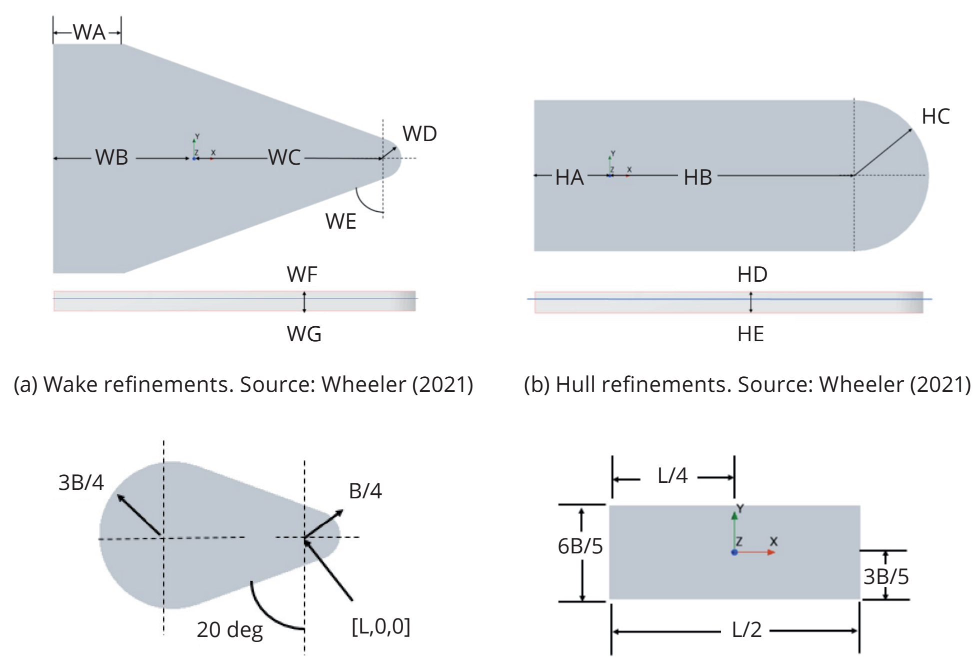

(a) Wake refinements. Source: Wheeler (2021)

(b) Hull refinements. Source: Wheeler (2021)

(c) Bow refinements. Source: Wheeler (2021)

(d) Stern refinements. Source: Wheeler (2021)

Fig. 6. General refinements for models A and B.

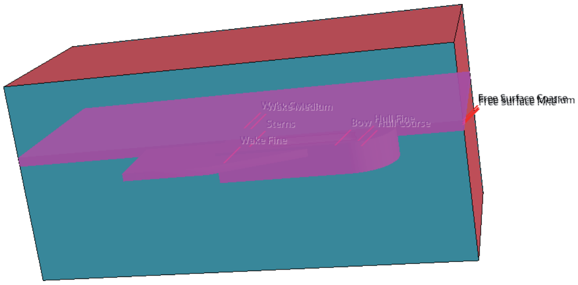

Fig. 7. Longitudinal view of the mesh with percentage refinement detail.

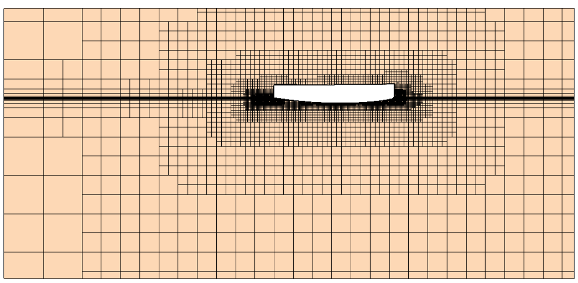

Fig. 8. Transverse view of the mesh with percentage refinement detail.

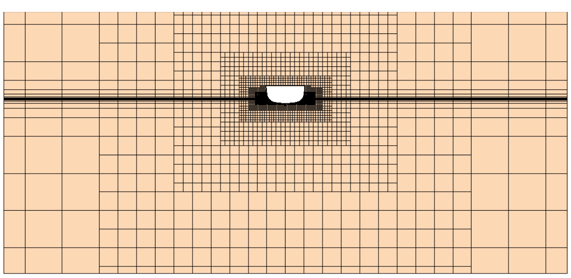

Boundary layer

The boundary layer is implemented along the hull surface, where viscous and pressure effects develop, which are important when obtaining the results of forces and flow characteristics. The formula used to calculate the thickness of the boundary layer:

$$y = \frac{y^{+} L_{mod}}{Re_L \times \sqrt{\frac{C_f}{2}}} \quad (1)$$

Where:

- y^+ = dimensionless parameter that is a measure of distance from the first grid cell to the surface.
- L_{mod} = model length hull
- Re_L = Reynold's number ($Re = VL/V$)
- C_f = Reynold's number (C_f=0,075 / $Log_{10}(Re_L$-2 $)^2$)

For this study, the authors have considered y^+ = 1, therefore.

Table 7. Boundary layer.

Parameter	Value
y+	1
Thickness of the first layer (*y*)	3.04×10^{-4}
Number of layers (*n*)	11
Stretch factor (*G*)	1.4
Boundary layer thickness (y_{total})	3.0×10^{-2}

The boundary layer calculation is fundamental for an accurate analysis of the physical phenomena that occur at the interface between the vessel and the fluid. The resulting boundary-layer thickness distribution is shown in Fig 9.

Fig. 9. Prism layer.

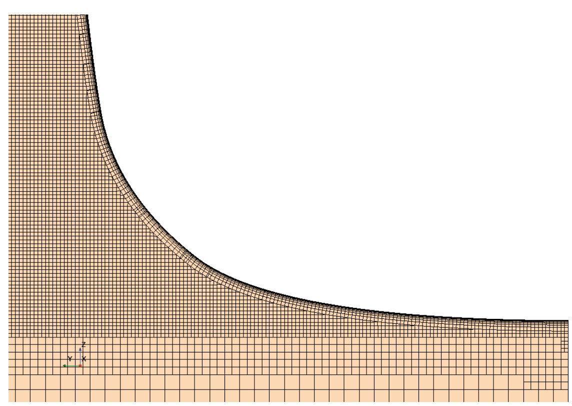

Turbulence models

Turbulence must be accurately modeled

due to its strong influence on hydrodynamic forces. This phenomenon consists of the irregular, random, and chaotic behavior of fluid particles in a given time and space. This unpredictable behavior makes it a complex phenomenon to study, which is why various researchers have tried to develop models to discretize it and provide applicable physical results. The three best-known turbulence models developed are DES, RANS, and DNS.

DNS (Direct Numerical Simulation) is a model that specializes in capturing rotating flows and vortices where the flow currents follow a circular or spiral path *(Richmond, 2019)*. A major limitation of DNS is its applicability to low-Reynolds-number flows and its high computational cost.

LES (Large Eddy Simulation) is a turbulence model that separates large from small turbulent structures in a physical phenomenon. The former, known as large scales, are composed of large vortices and are solved by the DNS model. The smaller vortices, known as small scales, are solved by a simplified, structured model known as a sub-mesh. This method combines the capabilities of DNS and RANS and represents flow vortices quite accurately.

Finally, for this study, the RANS (Reynolds Averaged Navier-Stokes) model was used. This model decomposes the flow velocity into an average velocity and a fluctuating velocity. While computationally more economical, it doesn't describe vortices as well as previous models, but it yields good results, especially considering its findings regarding frictional and pressure resistance of an object, making it ideal for this study.

RANS has developed two specific models: *k-ε* and *k-ω*. The former is widely used in industrial applications and, due to its low computational cost, is quite applicable, although it has some limitations in cases where adverse pressure gradients are significant. The *k-ω* model is much more sensitive but requires a higher computational cost.

In this work, the *k-ε* model was selected due to its computational efficiency; this model is used in many other works for similar case studies and has shown good applicability. Blazek (2005).

Physical and numerical configuration

The physical models selected for the simulation were:

Table 8. Physical models for ship model scale.

Group	Value
Time Group	Implicit Unsteady
Material Group	Multiphase
Multiphase Model Group	Volume of Fluid (VOF)
Viscous Regime Group	Turbulent
Reynolds-Averaged Turbulence Group	k-ε
Models Group	Gravity, Cell Quality Remediation y WOF Waves

The VOF Waves model allows the initial and boundary conditions of the waves to be specified, thus defining the condition of a plane wave.

Table 9. Properties of Flat VOF Wave on STAR-CCM+.

Property	Value	Units
Point On Water Level	[0.0, 0.0, 0.0]	m
Vertical Direction	[0.0, 0.0, 1.0]	m
Current	[-1.54/ -3.34 /-4.32, 0.0, 0.0]	m/s
Wind	[-1.54/ -3.34 /-4.32, 0.0, 0.0]	m/s
Light Fluid Density	1.1815	kg/m^3
Heavy Fluid Density	1025.00	kg/m^3

The tabulated values for Current and Wind represent an example case. In this study, these parameters were varied to evaluate the system's response to different flow and wind speeds.

Fig. 10. Free surface in flat state, with the volume fraction of water (blue) and air (red).

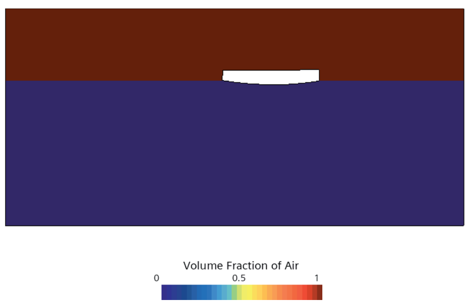

To avoid spurious reflections, numerical damping was applied at the boundaries, so STAR-CCM+ provides the VOF Wave Damping feature, which was activated at the boundaries by setting its value to 12m.

The boundary conditions were configured as shown in Table 10.

DFBI

DFBI (Dynamic Fluid Body Interaction) defines the motion and fluid–structure interaction of the body we define the body mass, center of gravity (CG), the radius of gyration (k_{xx}, k_{yy}, k_{zz}) about the CG, the release and ramp times,

Table 10. Boundary conditions properties configured on STAR-CCM++.

Variable	Values	Propertys
Input	Input speed	Velocity perpendicular to the surface with volume fraction of water and air applying damping effect.
Output	Outlet pressure	Water and air volume fraction, wave reflection by activated damping.
Hull	Wall	No displacement condition and smooth wall
Up	Input speed	Volume fraction of water and air. Movement velocity in x
Bottom	Input speed	Volume fraction of water and air. Movement velocity in x
Symmetry	Symmetry	Default
Deck y transom	Wall	No displacement condition ansmooth wall.
Side	Symmetry	Default. Applying Damping effect.

Fig. 11. Damping in Star CCM+. Figure (a) shows how waves form when numerical damping is not specified at the Input and Output, while (b) shows that it is specified and has a length of 9 m.

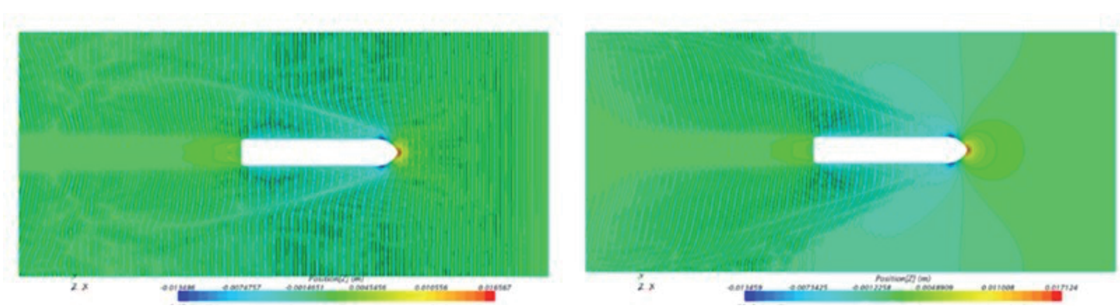

and the degrees of freedom enabled in the simulation (heave and pitch). Two vessels—Sailboat A and Sailboat B—are considered; their parameters are summarized in Tables 11 and 12. Unless otherwise stated, the body-fixed axes are aligned with the principal axes at the CG ($I_{xy} = I_{xz} = I_{yz} = 0$).

Table 11. DFBI properties for Sailboat A.

Property	Configuration
Body Surface	Sailboat A
Body Mass	7785 kg
Release Time	1.0 s
Ramp Time	5.0 s
Body Motion Option	Free Motion
Center of Mass (x, y, z)	[5.24, 0.0, 0.0] m
Radius of Gyration (k_{xx}, k_{yy}, k_{zz})	[1.365, 3.010, 0.457] m
Heave (Z)	Activated
Pitch (about Y)	Activated

Table 12. DFBI properties for Sailboat B.

Property	Configuration
Body Surface	Sailboat B
Body Mass	7785 kg
Release Time	1.0 s
Ramp Time	5.0 s
Body Motion Option	Free Motion
Center of Mass (x, y, z)	[5.464, 0.0, 0.0] m
Radius of Gyration (k_{xx}, k_{yy}, k_{zz})	[1.365, 2.897, 0.463] m
Heave (Z)	Activated
Pitch (about Y)	Activated

Stopping Criteria

The solution is composed of three parameters, which are the time step, the maximum number of iterations and the maximum physical time. The time step can be determined by the Courant number (which must be less than 1), represented by the following formula:

$$C = \frac{v\Delta t}{\Delta x} \qquad (2)$$

Where v is the fluid velocity, Δt is the passage of time and Δx is the length interval. In this study, Δx is defined as 0.05 meters, v is the maximum speed of the vessel and Δt is defined as 0.008. Therefore, $C_o = 0.691$

A maximum of 10 inner iterations per time step was es- tablished, a value consistent with similar CFD studies in naval hydrodynamics. The primary stopping criterion for the overall simulation was not a predefined duration, but rather the monitored stabilization of the total resistance force. Each simulation was run until the drag variable converged to a steady-state value with minimal oscillations. Consequently, this approach resulted in a different total physical time for each unique case, reflecting its specific hydrodynamic behavior as documented in the results (Table 14).

Results

This section evaluates the comparative hydrodynamic performance of Hull A and Hull B based on the CFD simulation results. To clearly illustrate the key findings, representative cases are presented graphically, focusing on the analysis of hull resistance, dynamic motions, and wave patterns.

Residuals

Numerical convergence for each simulation was verified using the residual plot. A simulation was considered successfully converged once the residual values for all governing equations dropped consistently below a target threshold of 1 × 100, indicating a stable numerical solution had been reached. This behavior is illustrated in Fig. 12.

DOI: 10.25043/19098642.282

Fig. 12. Residuals Type A sailboat - 6.50 kn Heel 15.00 Yaw 1.50.

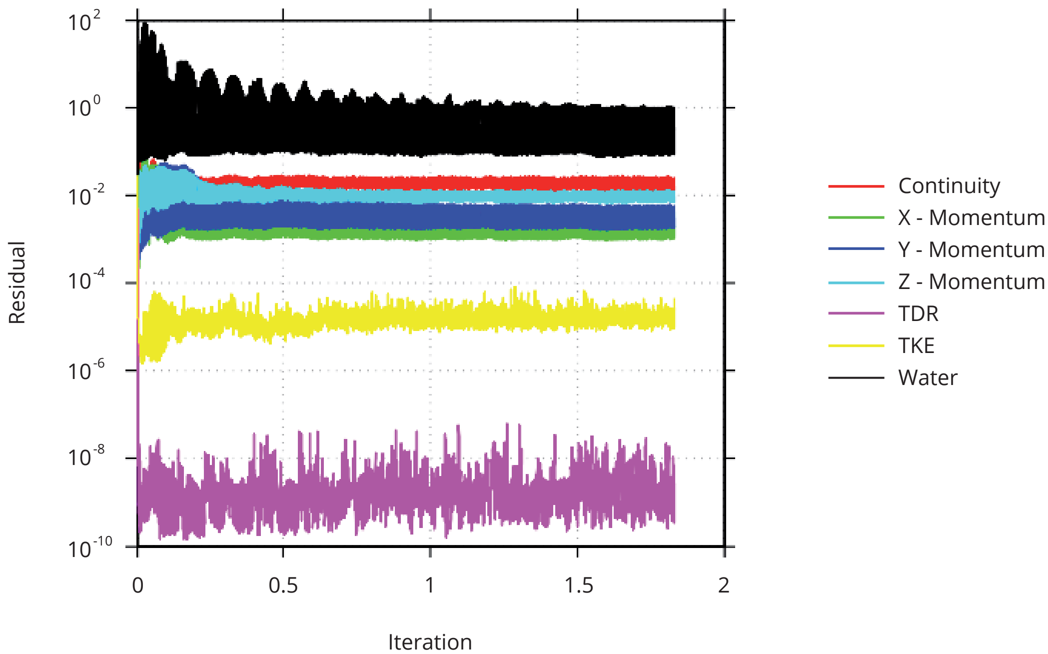

Table 13. Definition of residuals.

Residual	Description
Continuity	How much left to close the continuitequations.
x moment	Quantity movement in x axis.
y moment	Quantity movement in y axis.
z moment	Quantity movement in z axis.
TKE	Residuals referent to k parameter of the Reynolds average of the model turbulence k −ε.
TDR	Residuals of the Turbulent Dissipation Rate.
Water	Oscillation of water on the simulationgenerating wave system.

Drag Total

The comprehensive resistance results comparing both hull forms are summarized in Table 14. To provide a more detailed view of the hydrodynamic performance, Fig. 13 illustrates the convergence of the total resistance for a representative case, while Fig. 14 decomposes this total into its primary pressure and shear components. The data reveals a consistent trend where the normal bow (Hull A) experiences greater hydrodynamic resistance than the wide bow (Hull B) across all tested scenarios. For instance, at a top speed of 8.40 knots with zero heel and yaw, the total resistance for Hull A is 2546.91 N, which is 7.90 % higher than the 2360.24 N recorded for Hull B. This performance advantage for the wide bow is also observed under heeled conditions; at 6.50 knots with 15.00 degrees of heel, Hull A's resistance of 782.63 N remains slightly greater than Hull B's 770.30 N.

DFBI

The simulation captures an initial transient phase where the vessel seeks its dynamic equilibrium. When released, the hull quickly settles into its running attitude, experiencing a rapid increase in trim to a stable value of approximately 0.24 degrees (bow up) and a corresponding sinkage of about -0.01 meters. This initial adjustment period, is followed by a steady-state phase where both trim and sinkage remain constant, indicating that a stable hydrodynamic balance has been achieved.

Fig. 13. Drag Total Type A sailboat - 3.00 kn.

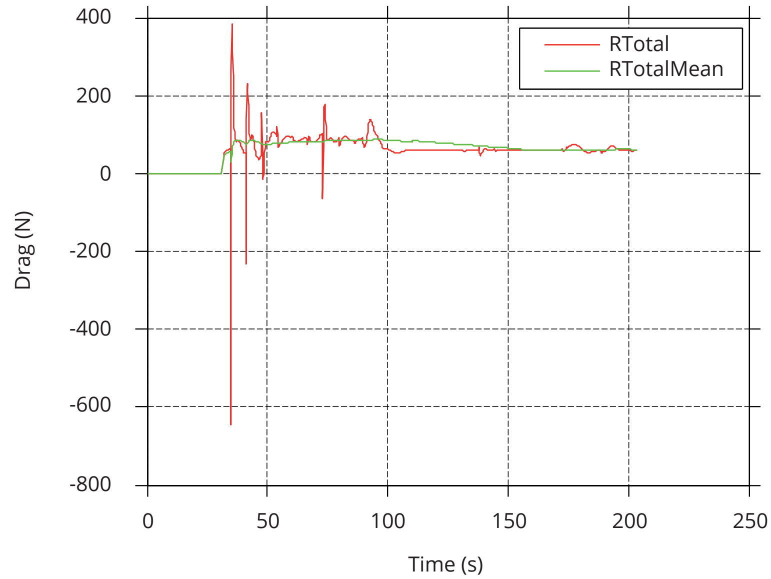

Fig. 14. Drag Pressure and Drag Shear vs Physycal Time - Type A sailboat - 3.00 kn.

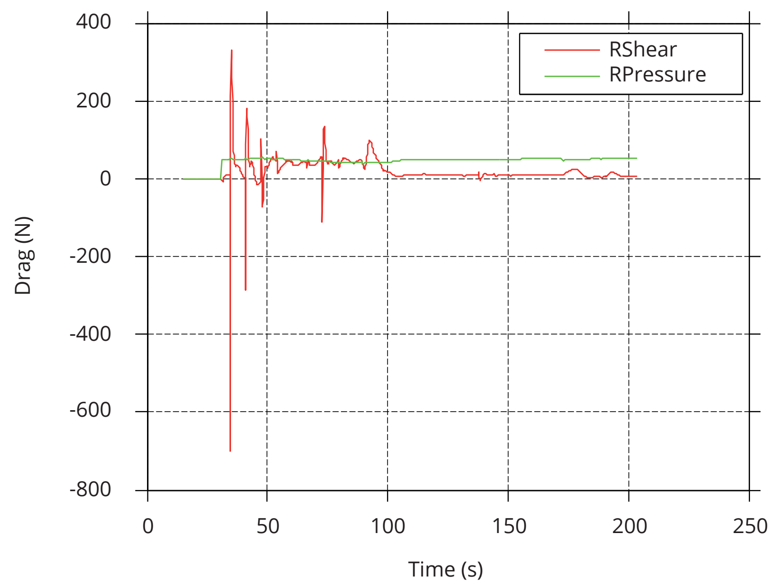

Table 14. Drag Total Results all simulations

(kn) V	(deg) Heel	(deg) Yaw	Drag Total A(N)	Drag Total B(N)	Diferences (N)
3.00	0.00	0.00	122.62	118.99	3.63
6.50	0.00	0.00	928.42	908.31	20.10
6.50	15.00	1.50	782.63	770.30	12.33
8.40	0.00	0.00	2546.91	2360.24	186.6
8.40	15.00	2.50	2401.09	2298.79	102.2

Fig. 15. Lift - Hull A 3.00 kn.

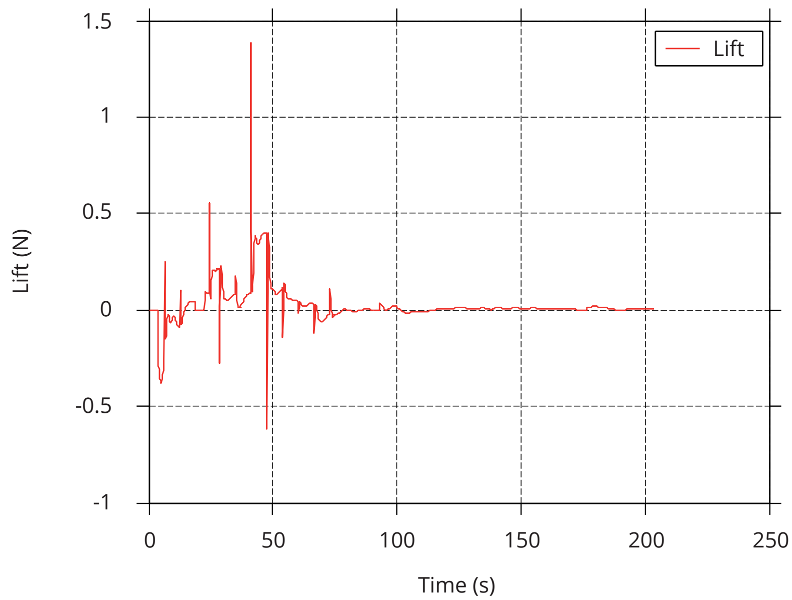

Fig. 16. Moment Y - Hull A 3.00 kn.

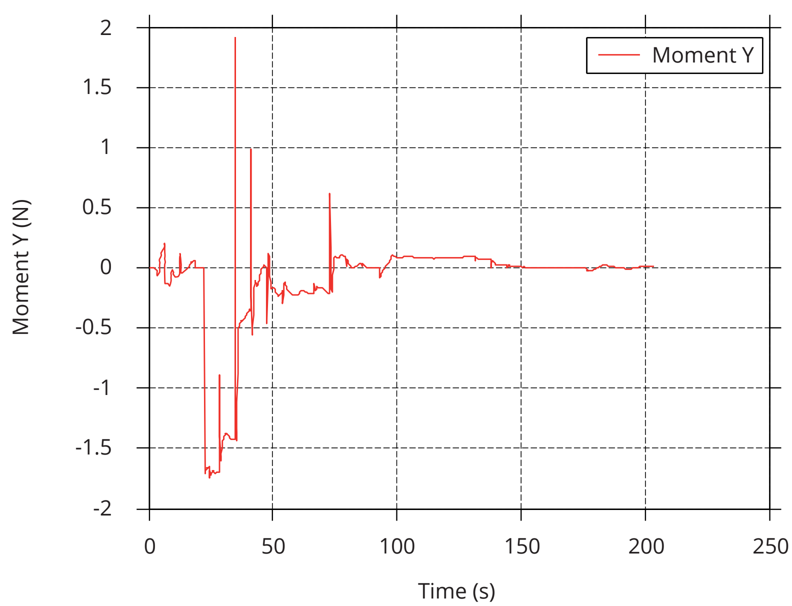

Solver CPU

The perfomance of the computer it shown in Fig. 18.

Waves

The wave pattern generated is shown in Fig. 19.

Wall Y$^+$

As illustrated in Fig. 21, the value of Y$^+$ is between 30 and 300.

Validation with Delft Series

A validation of the CFD methodology was

Fig. 17. Motion Monitor Hull A - 3.00 kn.

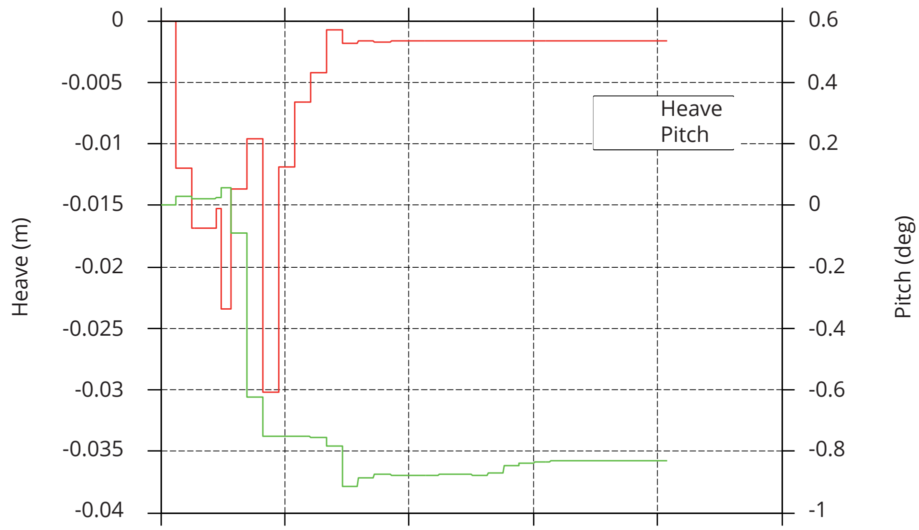

Fig. 18. Total Solver Elapsed Time Monitor.

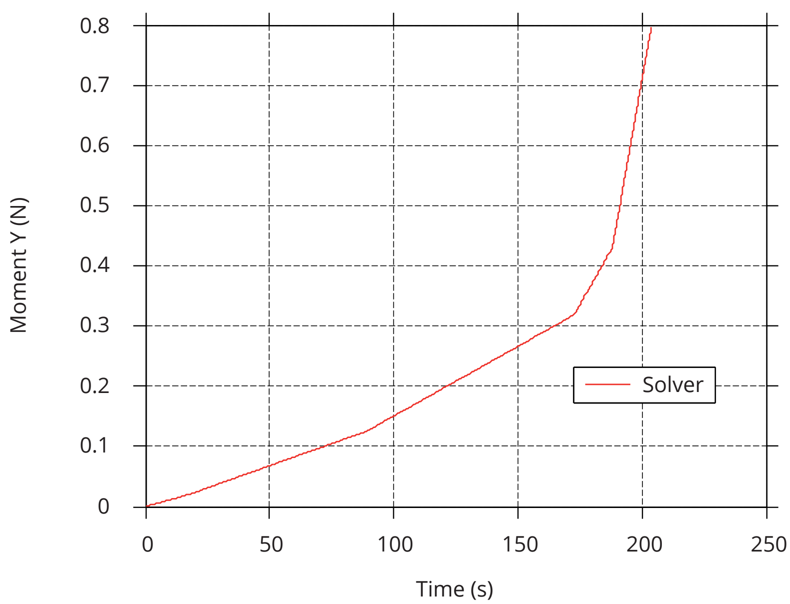

performed for the 6.50 knot case with a 0.00 degree heel and yaw by comparing the simulation results against the empirical data from the Delft Series I, II, and III, as illustrated in Table 15. The results show a consistent under-prediction by the CFD model, with the discrepancy ranging from 6.40% to 11.07% for Hull A and from 9.08% to 14.01% for Hull B when compared against the various Delft series datasets. This discrepancy is likely due to geometric differences between the simulated hulls and the Delft parent models, as well as the idealized conditions of the simulation.

Fig. 19. Wave pattern generated performed on STARCCM+ for Hull A - 8.4 kn.

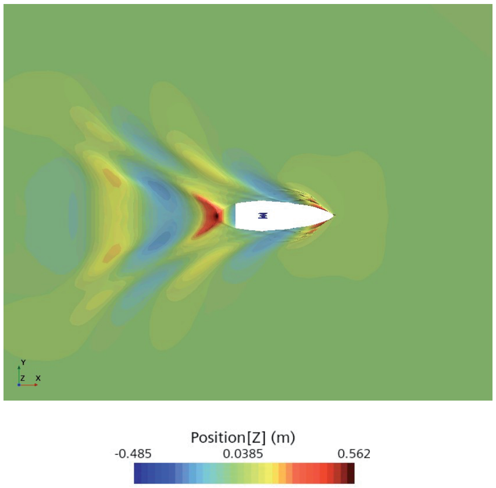

Table 15. Comparative Resistance Results for Hull A and Hull B.

Sailboat Type	Data Origin	Drag Total (N)
A	CFD Delft I, II Delft III	928,42 1044,04 991,91
B	CFD Delft I, II Delft III	908,32 1056,34 999,09

Fundamentally, the CFD simulation data agree that hull A exhibits greater resistance than hull B, but the Delft series presents a contradiction under these sailing conditions. This strong agreement in the qualitative performance trend validates the CFD setup and provides confidence in its use for comparative analysis of both hull types.

Conclusion

The CFD simulations conducted in this study demonstrate that the wide-bow hull (Hull B) exhibits superior hydrodynamic performance compared to the conventional-bow hull (Hull A), achieving total resistance reductions between **3.00% and 8.00%** under the evaluated conditions. For instance, at **8.40 knots without heel or yaw**, Hull B recorded a resistance of **2360.25 N**, compared to **2546.92 N** for Hull A, while at **6.50 knots with 15.00° heel**, resistance was also lower for Hull B (**770.30 N** versus **782.64 N**). This trend differs from the DSYHS data, which is expected because the systematic series does not account for differences in bow shape or wave-interaction effects does not take into account many shapes or surface-wave interactions, which supports the accuracy of the numerical model and reinforces the applicability of CFD as a predictive tool during the early and late stages of hull design. From a numerical standpoint, the numerical stability achieved, with residuals stabilized below **1×10^{-2}**, confirm the robustness of the method and its ability to reproduce complex hydrodynamic phenomena with high fidelity. From a practical standpoint,

Fig. 20. Wall Y^{+}.

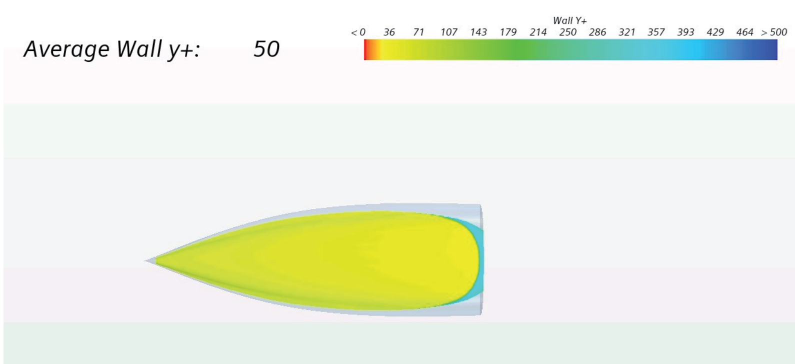

these results indicate that adopting wide-bow geometries in small craft design not only improves energy efficiency and reduces fuel consumption but also enhances operational stability and predictability across diverse conditions. This technical evidence supports the integration of wide-bow configurations in projects focused on performance optimization and improved seakeeping. Nevertheless, to strengthen the applicability of these findings to real-world conditions, it is recommended to complement numerical analyses with **scaled experimental testing and simulations in irregular waves**, thereby enabling the development of more robust and adaptable design criteria for a wider range of operational scenarios.

Contributions

- José S. Pájaro : Writing – original draft; Methodology; Data curation; Formal analysis; Software (STAR-CCM+); Visualization.
- Omar D Vásquez: Conceptualization; Investigation; Supervision; Writing – review & editing; Validation.

Funding source

This research received no external funding.

References

[1] BLAZEK, J., 2005. Chapter 7 - turbulence modelling, in: Blazek, J. (Ed.), Computational Fluid Dynamics: Principles and Applications (Second Edition). second edition ed.. Elsevier Science, Oxford, pp. 227–270. URL: https://www.sciencedirect.com/science/ article/pii/B9780080445069500096, doi:https://doi.org/10.1016/B978-008044506-9/50009-6.

[2] CASALONE, P., DELL'EDERA, O., FENU, B., GIORGI, G., SIRIGU, S., MATTIAZZO, G., 2020. Unsteady rans cfd simulations of sailboat's hull and comparison with full-scale test. Journal of Marine Science and Engineering 8, 394. doi:10.3390/jmse8060394.

[3] DOMÍNGUEZ RUIZ, F.J., GARCÍA JARAMILLO, L.A., TOWNSEND VALENCIA, P.R., 2020. Analysis of bow shapes proposed on a high-speed displacement hull, in: Carreño Moreno, V. (Ed.), Proceedings of CIDIN & COPINAVAL. Springer, pp. 89–103. doi:10.1007/978-3-030-35963-8_8.

[4] KAZEMI, H., DOUSTDAR, M.M., NAJAFI, A., NOWRUZI, H., AMERI, M.J., 2021. Hydrodynamic performance prediction of stepped planing craft using cfd and anns. Journal of Marine Science and Application 20, 67–84. doi:10.1007/s11804-020-00182-y.

[5] KEUNING, J.A., PINKSTER, J., VAN WALREE, F., 2002. Further in- vestigation into the hydrodynamic performance of the axe bow concept, in: Proceedings of the 6th Symposium on High Speed Marine Vehicles, University of Naples. pp. II.25–II.38.

[6] LARSSON, L., STERN, F., VISONNEAU, M., 2014. Numerical Ship Hydrodynamics: An Assessment of the Gothenburg 2010 Workshop. Springer, Dordrecht, Heidelberg, London, New York. URL: http://extras.springer.com, doi:10. 1007/978-94-007-7189-5. library of Congress Control Number: 2013948880.

[7] LIS´KIEWICZ, G., SOBCZAK, K., 2010. Cfd analysis of the sail interaction.

[8] LOPERA, O.D.A., 2019. Hydrodynamic Analysis of Inland Vessel Self-Propulsion for Cargo Transport for Navigability in The Magdalena River. Master's thesis.

Polytechnic School of the University of São Paulo. São Paulo.

[9] MATSUMOTO, A., HIROTA, K., YAMAGUCHI, H., 2019. Application of the design of experiments and computational fluid dynamics to bow design improvement. Journal of Marine Science and Engineering 7, 226. doi:10.3390/jmse7070226.

[10] MIYATA, H., AKIMOTO, H., HIROSHIMA, F., 1997. Cfd performance prediction simulation for hull-form design of sailing boats. Journal of Marine Science and Technology 2, 257–267. doi:10.1007/ BF02491532.

[11] ORTEGA, J.D.M., RODRÍGUEZ, J.M.R., 2024. Design of a self- righting pilot boat of 9 m length. Ship Science Technology (Cartagena) 18, 69–71. URL: https:// shipjournal. co/index.php/sst/article/ view/254, doi:10.25043/ 19098642.254.

[12] RIJKENS, A.A.K., MIKELIC, A., 2022. The hydrodynamic comparison between a conventional and an axe bow frigate hull, in: International Naval Engineering Conference (INEC), Delft University of Technology. pp. 1–18.

[13] S., P.J., 2022. Diseño conceptual de una barcaza autopropulsada con ruta barrancabermeja - cartagena para una futura hidrovía. Trabajo de grado presentado a la Facultad de Ingeniería para la obtención del Título de Ingeniero(a) Naval.

[14] SÁNCHEZ, W., VALDEZ, M., DÍAZ, J., GÓMEZ, C., DOMÍNGUEZ, F., 2025. Widening study of a 45-meter tuna fishing vessel based on multi-objective optimization. Ship Science Technology (Cartagena) 19, 34–37. URL: https:// shipjournal. co/index.php/sst/article/ view/272, doi:10.25043/ 19098642.272.

[15] WHEELER, M.P., 2021. Speeding up hydrodynamic simulations with a parametric, templated approach, in: Proceedings of the SNAME Maritime Convention, Society of Naval Architects and Marine Engineers, Providence, RI. pp. 1–10. URL: http://onepetro.org/ SNAMESMC/ proceedings-pdf/SMC21/2-SMC21/D021S004R002/ 2517635/sname-smc-2021-081.pdf.